Research in Astron. Astrophys. **????** Vol. **?** No. **XX**, 000–000
http://www.raa-journal.org *http://www.iop.org/journals/raa*

***R**esearch in*
***A**stronomy and*
***A**strophysics*

Key words: sun: activity — sun: photosphere — sun: magnetic field

A Brief Report on Statistical Study of Net Electric Current in Opposite Polarity Longitudinal Field Area of Solar Active Regions

Y. Gao[1]
Key Laboratory of Solar Activity, National Astronomical Observatories, National Astronomical Observatories, Chinese Academy of Sciences, Beijing 100012, China; *gy@bao.ac.cn*

Received [year] [month] [day]; accepted [year] [month] [day]

Abstract The dynamic process of solar active regions is dominated by the solar magnetic field. As of now, the observation has supplied us the vector components of solar photospheric magnetic field with the solar magnetograph. The two transverse components of photospheric magnetic field allow us to compute the quantity of electric current. It is found that the electric current in the positive (negative) polarity longitudinal magnetic area have both signs in a sunspot, however, the net current is found to be an order-of-magnitude less than the mean absolute magnitude and has a preferred sign. In particular, the net electric current is positive (negative) in negative (positive) magnetic polarity in the northern (southern) hemisphere, though in the solar minimum the tendency is reversed in some latitudinal-time bins. The result indicates that there is weak net electric current in the opposite polarity area of the solar active regions, and thus, it supplies further details of the hemispheric helicity rule found in a series of previous studies.

1 INTRODUCTION

In the solar atmosphere, it has been found a chirality of photospheric magnetic field of active regions that usually manifested by the parameter of current helicity or force free field factor. In the Northern (Southern) solar hemisphere, the helicity possess statistically and mainly left (right) handedness, which was called hemispheric helicity sign rule (Seehafer 1990; Pevtsov et al. 1994; Pevtsov et al. 1995; Abramenko et al. 1996; Bao & Zhang 1998; Hagino & Sakurai 2004; Zhang et al. 2010). Furthermore, the helicity sign distribution is further investigated in between the 23^{rd} and 24^{th} solar activity cycle (e.g., Hao & Zhang 2012). Generally, both left and right handedness on a particular pixel coexist in an image of solar active region or even a sunspot when deriving with a solar vector magnetogram. The physical explanation of the hemispheric helicity sign rule is still a complicated problem. Some typical case analyses showed that there was opposite net current system in several active regions (Wang, Xu & Zhang 1994; Leka et al. 1996; Wang & Abramenko 1999; Wheatland 2000). However, it is also inferred that there was no net current in the sunspot (Venkatakrishnan & Tiwari 2009). The application of the parameter of current helicity in the active regions become suspect again. In this paper, we try separating the positive and negative flux area according to the longitudinal field of solar active region and study the distribution of the current.

2 OBSERVATIONS

Vector magnetograms observed by the Solar Magnetic Field Telescope (SMFT), that is a tunable birefringent filter-type video vector magnetograph (Ai 1987). For photospheric observations the passband

of the filter is set in the FeI λ5324 Å. Normally the longitudinal component of field (Stokes V) is measured at -75 mÅ and the transverse components (Stokes Q and U) are measured at the line core. The equivalent width of FeI λ5324 Å line is 0.344 Å and the FWHM of the filter passband is 0.15 Å. Vector magnetograms are reconstructed by the following relations,

$$B_{\parallel} = C_{\parallel} \frac{V}{I} \tag{1}$$

$$B_{\perp} = C_{\perp} \left[\left(\frac{Q}{I}^2 + \frac{U}{I}^2 \right) \right]^{1/4} \tag{2}$$

in which $C_{\parallel}$ and $C_{\perp}$ are the calibration coefficients for the longitudinal and transverse fields (Su & Zhang 2004). The azimuth of the transverse field is

$$\phi = \frac{1}{2} \arctan \left(\frac{U}{Q} \right) \tag{3}$$

Thus the y- and x- components of the vector magnetic field are as following:

$$B_y = B_{\perp} \sin \phi \tag{4}$$

$$B_x = B_{\perp} \cos \phi \tag{5}$$

The 180° ambiguity resolution of the transverse field is carried out following Wang et al. (1994) by comparison with the potential field. The active regions under investigation are all located near the center of the disk. The latitude and longitude are less than 40°, so that the projection effects are small. Therefore we may denote the line-of-sight and horizontal components of magnetic field as B_z and B_t, respectively. Usually, in our computations, we select the pixels where the signal exceeds the noise levels $|B_z| > 20G$ and $B_t > 100G$. The different reduction with the previous research is that we compute the average value of J_z ($\langle J_z \rangle$) on the pixels where ($B_z > 20G$, $B_t > 100G$) and ($B_z < -20G$, $B_t > 100G$) respectively. The derived parameter is longitudinal electric current, which is defined as $J_z = (1/\mu_0)(\partial B_y/\partial x - \partial B_x/\partial y)$.

3 DATA REDUCTION

3.1 Case of NOAA 10484

Figure 1 shows a simple relation of the electric current with the pixel positions. The top panel shows the electric current in both the positive and negative longitudinal field areas of the active region NOAA 10484. The middle and bottom panels show the electric current in the positive and negative longitudinal field area respectively. Compared with the top panel, the latter two show a weak negative and positive deviation of electric current in spite of standard deviations of same order.

Figure 2 shows the detailed information on the distribution of the electric current of NOAA 10484. The vector magnetogram is observed on 09:49:42 of Oct-22, 2003. There are three Columns in Figure 1, the first Column shows the distribution of electric current in the both positive and negative longitudinal field area. The grey patterns in Row 2 - 5 show the J_z in the interval of an order-of-magnitude varying from 10^0 to 10^{-4} respectively. The pixel numbers where $|J_z| > 10^0 A$ account for 2.5%. The pixel numbers where $|J_z| < 10^{-3} A$ account for 57%, however, the $\langle |J_z| \rangle$ is only on the order of 10^{-5}. The main contribution of $\langle |J_z| \rangle$ are of the order-of-magnitude of 10^{-3} - $10^0 A$, as shown in the Row 2 - 4 of the first Column.

The second Column shows the distribution in the positive longitudinal field area. It is found that a mean current -1.61 $\times 10^{-2} A$, -1.68 $\times 10^{-2} A$ and -2.96 $\times 10^{-4} A$ compared to the mean absolute magnitude of 5.13 $\times 10^{-2} A$, 4.46 $\times 10^{-2} A$ and 3.05 $\times 10^{-3} A$ below the order of 10^0, 10^{-1} and $10^{-2} A$, respectively.

The third Column shows the distribution in the negative longitudinal field area. It is found that a mean current 1.69 $\times 10^{-2} A$, 3.43 $\times 10^{-3} A$ and -4.95 $\times 10^{-4} A$ compared to the mean absolute magnitude of 9.74 $\times 10^{-2} A$, 6.34 $\times 10^{-2} A$ and 3.36 $\times 10^{-3} A$ below the order of 10^0, 10^{-1} and $10^{-2} A$, respectively.

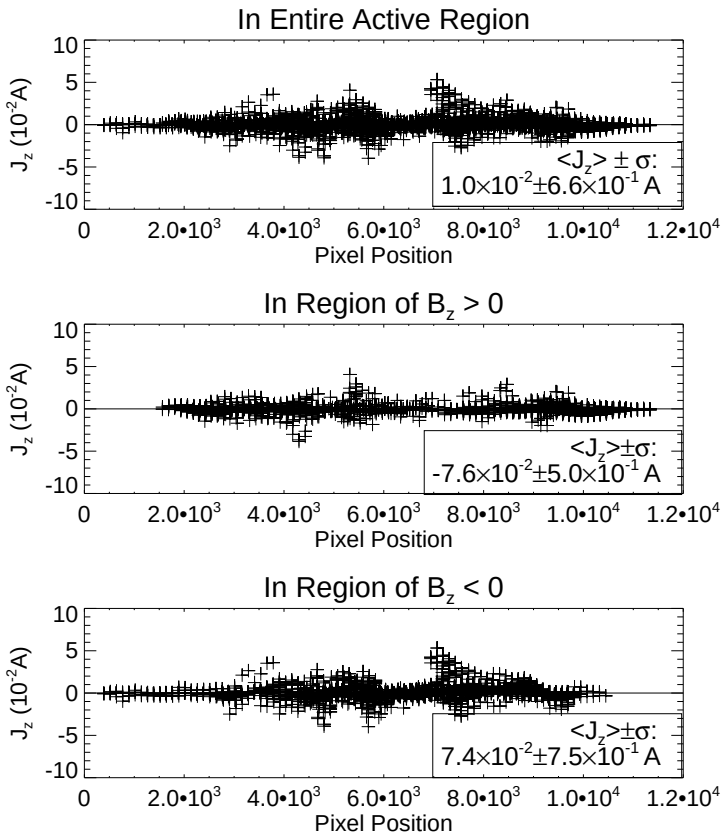

Fig. 1 Electric current as a function of pixel position. The top panel shows the electric current in both positive and negative longitudinal field areas of the active region NOAA 10484. The middle and bottom panels show the electric current in the positive and negative longitudinal field area respectively.

3.2 Statistic Study of Large Sample

We do analysis at the base of 6629 vector magnetograms observed at Huairou Solar Observing Station from 1988 to 2005. The detailed information is referred to Zhang et al. (2010). The effective field of view (FOV) is $5.23' \times 3.63'$ (Before Aug-25, 2001), $4.06' \times 2.77'$ (Aug-25, 2001 to Oct-13, 2001 and Oct-14 to Nov-30, 2001) and $3.75' \times 2.81'$ (After Dec-1, 2001). After obtaining $\langle J_z \rangle$ on each magnetogram, we compute the 2-year running average in the 7° latitudinal interval. Then we obtain butterfly diagrams shown in the figure 3.

Figure 3 shows that the $\langle J_z \rangle$ is negative (positive) in the positive (negative) longitudinal field area of active regions in the northern (southern) hemisphere in most bins. The colorful background is the butterfly diagram of sunspot area. The vertical color bar beside the upper (bottom) panel indicates the leading polarity is mainly negative (positive) and the following polarity is mainly positive (negative). So the whole butterfly diagram tells us the weak net current points from the negative (positive) polarity to the positive (negative) polarity sunspot in the northern (southern) hemisphere statistically. Additionally, there are obvious exceptions in the minimum of solar activity cycle. It implies that the reversal sign helicity in the minimum of the solar activity cycle is an intrinsic property of evolution of solar magnetic field. It should be pointed out that the exceptions are found in not only the minimum but also the whole

solar activity cycle. The ratio of exceptions is relatively higher in the minimum than other phases of the solar cycle.

Figure 4 shows two exceptions. The upper panels show the vector magnetogram of NOAA 9690 (Left) and the distribution of electric current which order-of-magnitude is less than $10^0 A$ (Right). The $\langle J_z \rangle$ is $-1.22 \times 10^{-2} A$ compared to the $\langle |J_z| \rangle$ of $1.08 \times 10^{-1} A$ (11.3%). The bottom panels show the vector magnetogram of NOAA 8675 (Left) and the distribution of electric current which order-of-magnitude is less than $10^0 A$ (Right). The $\langle J_z \rangle$ is $-2.06 \times 10^{-3} A$ compared to the $\langle |J_z| \rangle$ of $1.86 \times 10^{-2} A$ (11.1%).

4 CONCLUSIONS AND DISCUSSION

It has been found that the systematic net electric current of the negative (positive) polarity in the positive (negative) polarity area of solar active regions in the northern (southern) hemisphere statistically. The tiny net electric current ($\langle J_z \rangle$) is an order-of-magnitude smaller than the mean absolute magnitude of electric current $\langle |J_z| \rangle$ in the whole active region. It supplies more details of the hemispheric helicity sign rule found by a series of previous studies. For example, the net current in the positive (negative) polarity area of solar active regions in the northern (southern) hemisphere is statistically negative, as a result, they will cause an excess negative (positive) current helicity in the northern (southern) hemisphere, thus is consistent with the sign preference of the hemispheric helicity sign rule.

In the minimum of solar activity cycle, it is found some exceptions of net electric current which has an opposite direction with reference to the normal ones. It supplies a self-consistent evidence that the reversal sign of helicity observed based on Huairou Solar Observing Station reflect the intrinsic property of solar magnetic field twist. Furthermore, we compute the ratio of active regions conforming or not conforming the hemispheric helicity sign rule. As the Table 1 shows, bolded fonts show the conforming ones. Besides weak preference of sign, there are some unusual features, too. For the 22^{nd} solar cycle, the ratios are 67.6% (61.9%) when $B_z > 0$ ($B_z < 0$) in the southern (northern) hemisphere. The ratios are higher than 51.6% (46.3%) when $B_z < 0$ ($B_z > 0$) in the southern (northern) hemisphere. For the 23^{rd} solar cycle, the ratios of sign-preferred active regions are 62.7% (67.8%) when $B_z > 0$ ($B_z < 0$) in the southern (northern) hemisphere. The ratios are still higher than 51.1% (53.1%) when $B_z < 0$ ($B_z > 0$) in the southern (northern) hemisphere. This imbalance of net current in different hemisphere when $B_z < 0$ or $B_z > 0$ may arise from the effect of Faraday rotation, which can cause excess false positive net current in an active region (Hagino and Sakurai, 2004; Gao et al., 2008). Nevertheless, the areas of negative current in the southern (northern) hemisphere of $B_z > 0$ ($B_z < 0$) show convincing features to support the reversal sign helicity is independent with the effect of Faraday rotation. Although the hemispheric helicity sign rule holds over the whole 23^{rd} solar activity cycle, the apparent areas of reversal sign are seen in the southern hemisphere at the end of the cycle. It is in agreement with another statistical analysis done by Hao and Zhang (2010) with independent data observed by Hinode in the descending phase of 23^{rd} solar activity cycle.

Acknowledgements I am grateful to the referee for helpful comments and suggestions. The work is supported by the National Natural Science Foundation of China under grants 11273034, 11178005, 41174153, 11173033, 11103037, National Basic Research Program of China under grant 2000078401 and 2006CB806301, and Chinese Academy of Sciences under grant KJCX2-EW-T07.

References

Abramenko, V. I., Wang, T. J. & Yurchishin, V. B. 1996, *Solar Phys.*, 168, 75
Ai, G. 1987, Publ. Beijing Astron. Obs., No 9, 27-36
Bao, S. D. & Zhang, H. Q. 1998, *ApJ*, 496, L43.
Gao, Y., Su, J.; Xu, H. & Zhang, H. 2008, *MNRAS.*, 386., 1959G.
Hagino, M. & Sakurai, T. 2004, *PASJ*, 56, 831.
Hao, J. & Zhang, M. 2012, *ApJ*, 733, L27.

Hemisphere	($\langle J_z \rangle > 0$, $B_z > 0$)	($\langle J_z \rangle < 0$, $B_z > 0$)	($\langle J_z \rangle > 0$, $B_z < 0$)	($\langle J_z \rangle < 0$, $B_z < 0$)
		22^{nd} cycle		
North	53.6%	**46.3%**	**61.9%**	38.1%
South	**67.6%**	32.4%	48.4%	**51.6%**
		23^{rd} cycle		
North	48.9%	**51.1%**	**67.8%**	32.3%
South	**62.7%**	37.3%	46.9%	**53.1%**

Table 1 The ratios of active regions conforming (Bolded fonts) and not conforming the hemispheric helicity sign rule.

Leka, K. D., Canfield, R. C., McClymont, A. N. & van Driel-Gesztelyi, L. 1996, *ApJ*, 462, 547.
Pevtsov, A. A., Canfield, R. C. & Metcalf, T. R. 1994, *ApJ*, 425, L117.
Pevtsov, A. A., Canfield, R. C. & Metcalf, T. R. 1995, *ApJ*, 440, L109.
Seehafer, N. 1990, *Solar Phys.*, 125, 219.
Su, J. T. & Zhang, H. 2004, *Chinese Astronomy and Astrophysics*, **4**, 365;
Venkatakrishnan, P. & Tiwari, S. K. 2009, *ApJ*, 706, L114.
Wheatland, M. S. 2000, *ApJ*, 532, 616.
Wang, T. J., Xu, A. A. & Zhang H. Q. 1994, *Solar Phys.*, 155, 99.
Wang, T. J. & Abramenko, V. A. 1999, *ESASP.*, 448, 671.
Zhang, H. Q., Sakurai, T., Pevtsov, A., Gao, Y., Xu, H. Q., Sokoloff, D. D. & Kuzanyan, K. 2010, *MNRAS*, 402L, 30.

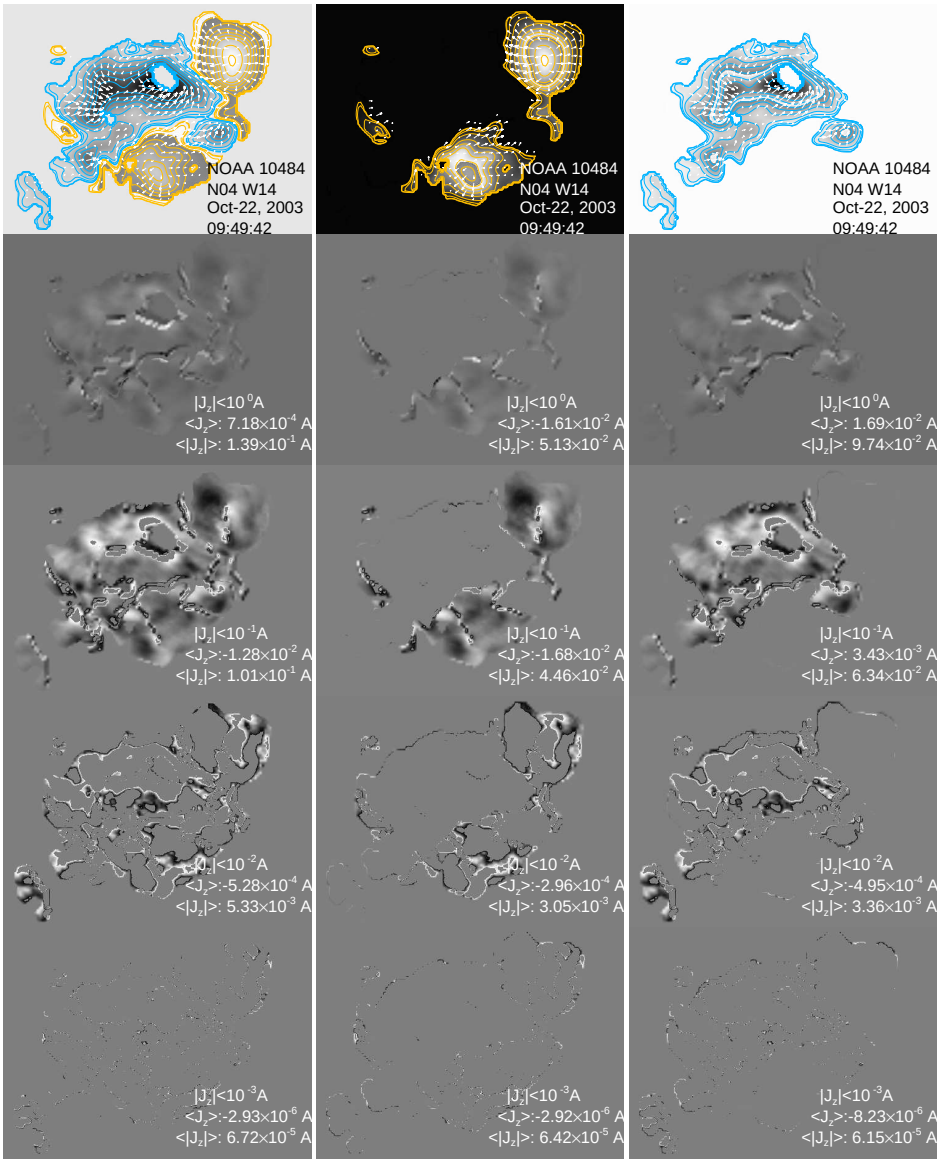

Fig. 2 The top panels in each column shows the original vector magnetogram and the grey-scale image shows the longitudinal magnetic field of NOAA 10484. The orange (cyan) contour show the positive (negative) longitudinal magnetic field. The contour level is [±30.,160.,480.,800.,1280.,1600G]. The first Column shows the distribution of electric current in both positive and negative longitudinal field areas. The second Column shows the distribution in the positive longitudinal field area. The third Column shows the distribution in the negative longitudinal field area. The grey-scale images from the second to five rows show the electric current. The corresponding scale of magnitude is shown in the each right bottom corner.

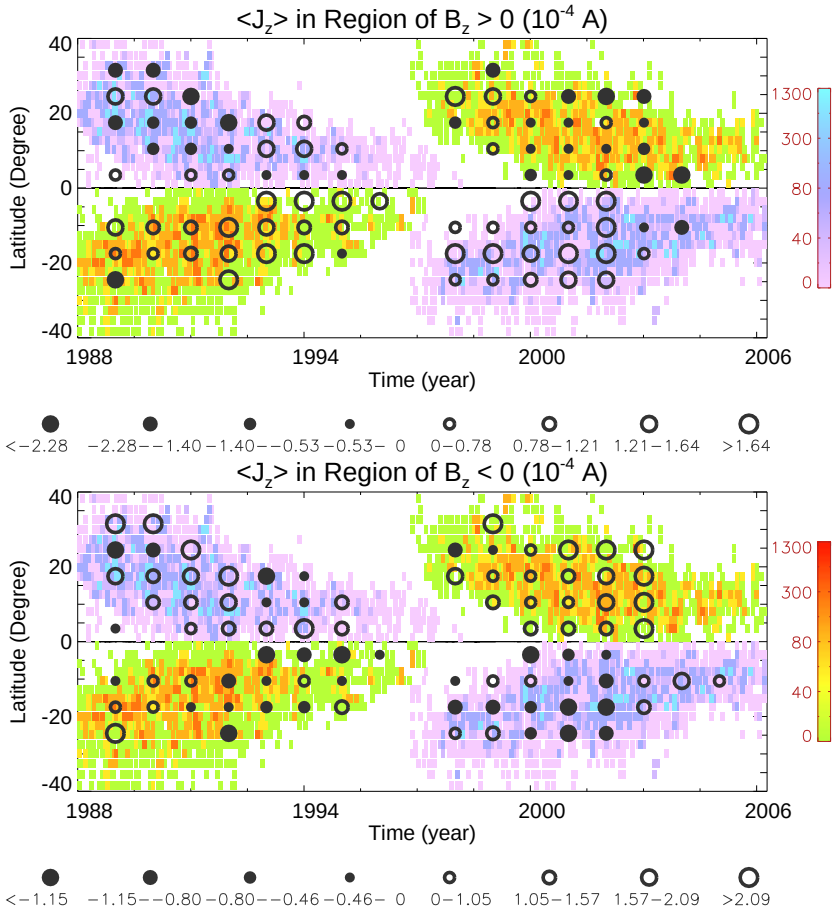

Fig. 3 The circle (filled circle) show the positive (negative) sign of the mean electric current. The circle sizes give the magnitude of the displayed quantity. Superimposed, the underlying colored "butterfly diagram" shows how sunspot density varies with latitude over the solar cycle. The upper (bottom) vertical color bar on the right stands for the leading sunspot of negative (positive) polarity.

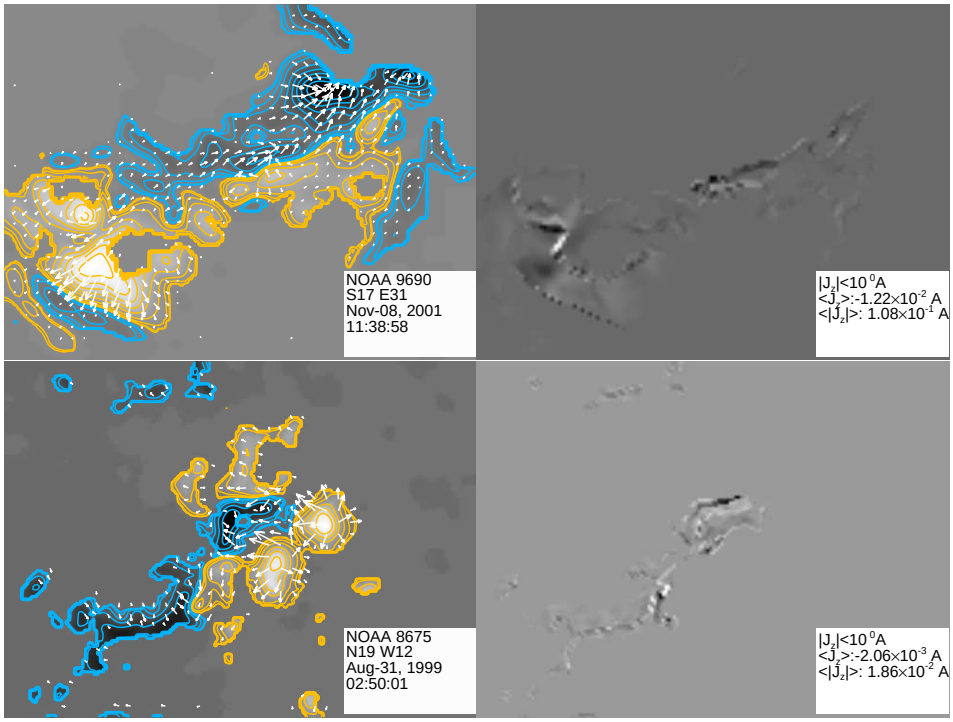

Fig. 4 The upper panels show the vector magnetogram of NOAA 9690 (Left) and the distribution of electric current on the positive polarity area (Right). The bottom panels show the vector magnetogram of NOAA 8675 (Left) and the distribution of electric current on the negative polarity area (Right).